

Limit-Cycle Behaviour of Thermally-Unstable Accretion Flows onto Black Holes

Ewa Szuszkiewicz^{1,2} and John C. Miller^{2,3}

¹*Astronomy Group, Department of Physics and Astronomy, University of Leicester, University Road, Leicester LE1 7RH*

²*International School for Advanced Studies, SISSA, via Beirut 2-4, I-34013 Trieste, Italy*

³*Nuclear and Astrophysics Laboratory, University of Oxford, Keble Road, Oxford OX1 3RH*

19 March 2018

ABSTRACT

Nonlinear time-dependent calculations are being carried out in order to study the evolution of vertically-integrated models of non-selfgravitating, transonic accretion discs around black holes. In this paper we present results from a new calculation for a high- α model similar to one studied previously by Honma, Matsumoto & Kato who found evidence for limit-cycle behaviour connected with thermal instability. Our results are in substantial agreement with theirs but, in our calculation, the disc material does not always remain completely optically thick and we include a suitable treatment for this. We followed the evolution for several cycles and determined the period of the cycle as being about 780 seconds. Advective cooling is dominant in the region just behind the outward-moving peak of surface density. The behaviour of this model is significantly different from what we saw earlier for low- α models (which we discussed in a previous paper) and we contrast and compare the two situations.

Key words: accretion: accretion discs – instabilities: thermal

1 INTRODUCTION

Accretion discs can be subject to thermal instability (Pringle, Rees & Pacholczyk 1973) but occurrence of an instability does not necessarily mean that after the characteristic growth-time, the disc will be disrupted. The instability may also saturate in the non-linear regime giving rise to continuing non-stationary behaviour of the system. This may well be what is

happening in the X-ray source GRS 1915+105 which has shown a remarkable richness in its variability behaviour (Belloni et al. 1997).

In a previous paper (Szuszkiewicz & Miller 1997 – hereafter Paper I) we reported on the first stages of a programme to investigate the evolution of the thermal instability in vertically-integrated models of non-selfgravitating, transonic accretion discs around black holes. It was found that for the original version of the slim-disc model (Abramowicz, Czerny, Lasota & Szuszkiewicz, 1988) with low viscosity ($\alpha = 0.001$), the instability led to formation of a shock-like structure near to the sonic point which, in the absence of special treatment, led to termination of the calculation. This was very different from the behaviour reported by Honma, Matsumoto & Kato (1991, hereafter HMK) for a basically similar model having the viscosity parameter α two orders of magnitude larger.

The aim of the present paper is to investigate a model with high α , similar to the one studied by HMK, following the same mathematical and numerical approach as in Paper I, so as to clarify whether there is a genuine difference between the low and high α regimes. The parameter values used are the same as those chosen by HMK: $M = 10M_{\odot}$, $\dot{M} = 0.06 \dot{M}_{cr}$ and $\alpha = 0.1$ although the resulting model is slightly different from theirs because of the different mathematical formulation adopted. (\dot{M}_{cr} is the critical accretion rate corresponding to the Eddington luminosity.) We find behaviour which is qualitatively similar to that presented by HMK and decisively different from the low- α case. In our calculations we obtained closed paths in the $\log T - \log \Sigma$ plane and followed the evolution for three full cycles. In the short outburst phase the assumption of the gas being optically thick is not fully satisfied and so we have introduced an appropriate treatment for dealing with this and recalculated the whole evolution.

The plan of the paper is as follows. In Section 2 we summarize the basic equations used in the calculations and introduce the treatment adopted for dealing with the medium when it is not optically thick. In Section 3, we present the global behaviour and phase space portraits as derived from our calculations. The present results are compared with those of HMK in Section 4 which also contains a discussion of the difference between the low and high α cases. Section 5 is the conclusion.

2 BASIC EQUATIONS

The equations used to describe the evolution of the thermal instability in an axisymmetric, non-self-gravitating, optically-thick disc have been presented in full detail in Paper I and here we just list them again for completeness while describing in more detail the treatment which we have used for the part of the flow which is not optically thick.

In cylindrical polar coordinates (r, φ, z) centered on the black hole (having mass M), our basic hydrodynamical equations for conservation of mass, energy and momentum are as follows:

$$\frac{D\Sigma}{Dt} = -\frac{\Sigma}{r} \frac{\partial}{\partial r} (rv_r) \quad (1)$$

$$\frac{Dv_r}{Dt} = -\frac{1}{\rho} \frac{\partial p}{\partial r} + \frac{(l^2 - l_K^2)}{r^3} \quad (2)$$

$$\frac{Dl}{Dt} = -\frac{\alpha}{r\Sigma} \frac{\partial}{\partial r} (r^2 p H) \quad (3)$$

$$\Omega_K^2 H^2 = 6 \frac{p}{\rho} \quad (4)$$

$$\rho T \frac{DS}{Dt} = Q_{vis} + Q_{rad}, \quad (5)$$

Here, D/Dt is the Lagrangian derivative given by

$$\frac{D}{Dt} = \frac{\partial}{\partial t} + v_r \frac{\partial}{\partial r}, \quad (6)$$

$\Sigma = \Sigma(r, t)$ is the surface density obtained by vertically integrating the mass density ρ , H is the half-thickness of the disc, $v_r = Dr/Dt$ (which is negative for an inflow), p is the pressure, $l = l(r, t) = rv_\varphi(r, t)$ is the specific angular momentum, l_K is the value of l for Keplerian motion with $v_\varphi = [GMr/(r - r_G)^2]^{1/2}$, $\Omega_K = v_\varphi/r$, S is the entropy per unit mass, T is the temperature, Q_{vis} is the rate at which heat is generated by viscous friction

$$Q_{vis} = -\alpha p r \left(\frac{\partial \Omega_K}{\partial r} \right), \quad (7)$$

and Q_{rad} is the rate at which heat is lost or gained by means of radiative energy transfer

$$Q_{rad} = -\frac{F^-}{H} \quad (8)$$

with F^- being the radiative flux away from the disc in the vertical direction for which we use the expression

$$F^- = \frac{16\sigma T^4}{\kappa\rho H}, \quad (9)$$

where σ is the Stefan-Boltzmann constant and κ is the opacity. (Note that this expression is

the same as that used for F^- in Paper I but written in terms of σ rather than the radiation constant a .)

The thermodynamic quantities in the equatorial plane are taken to obey the equation of state

$$p = k\rho T + \frac{a}{3}T^4 \quad (10)$$

and the opacity is approximated by the Kramers formula for chemical abundances corresponding to those of Population I stars

$$\kappa = 0.34(1 + 6 \times 10^{24} \rho T^{-3.5}) \text{ g}^{-1} \text{ cm}^2. \quad (11)$$

If the medium is not optically thick, the diffusion approximation from which the radiative flux equation (9) was derived is no longer valid. Following Huré et al (1994) (see also Lasota & Pelat (1991); Narayan & Yi (1995) and Artemova et al. (1995)) we have then adopted a general formula for F^- based on the solution proposed by Hubeny (1990) in the Eddington approximation:

$$F^- = 6 \frac{4\sigma T^4}{\frac{3\tau_R}{2} + \sqrt{3} + \frac{1}{\tau_P}} \quad (12)$$

where τ_R and τ_P are the Rosseland and Planck mean optical depths (equal to $\kappa_R \rho H$ and $\kappa_P \rho H$). The expression for the radiation pressure corresponding to this F^- is

$$P_r = \frac{F^-}{12c} \left(\tau_R + \frac{2}{\sqrt{3}} \right) \quad (13)$$

In the optically-thick limit τ_R and τ_P are much larger than unity and formulae (12) and (13) reduce to the standard expressions for F^- and P_r . The terms involving τ_R are dominant here whereas in the opposite optically-thin limit, they are negligibly small compared with other terms and $1/\tau_P$ becomes the dominant contribution to the denominator of (12). Formulae (12) and (13) provide a convenient interpolation between the two limits. The expressions used for τ_R and τ_P need to give reasonable results in the two limits. Here we adopt a very simple treatment. For the Rosseland optical depth, we use the expression

$$\tau_R = 0.34 \Sigma (1 + 6 \times 10^{24} \rho T^{-3.5}), \quad (14)$$

corresponding to the κ given by equation (11), while for the Planck optical depth we use

$$\tau_P = \frac{1}{4\sigma T^4} (q_{br}^-) \quad (15)$$

where q_{br}^- is the bremsstrahlung cooling rate given by

$$q_{br}^- = 1.24 \times 10^{21} H \rho^2 T^{1/2} \text{ erg cm}^{-2} \text{ s}^{-1} \quad (16)$$

Of course, bremsstrahlung is only one of the important processes contributing to the Planck opacity and it is our intention to include others in future work.

3 RESULTS FOR THE HIGH- α MODEL

As mentioned in the Introduction, we are here focusing attention on a particular model with black hole mass $M = 10M_{\odot}$, initial accretion rate $\dot{M} = 0.06\dot{M}_{cr}$ and viscosity parameter $\alpha = 0.1$. These parameters are the same as those used by HMK for their model having the viscous stress component $\tau_{\varphi r}$ proportional to the total pressure ($q = 0$ in their notation) but our model is not completely identical to theirs because of the different formulations used. In this section, we give a detailed presentation of the results which we have obtained and delay until Section 4 comments on the comparison with those of HMK.

Our computations were carried out using the Lagrangian hydrodynamics code described in detail in Paper I. The grid organization and spacing were similar to before but this time it was necessary to extend the grid out to larger values of r in order for conditions in the neighbourhood of the outer boundary to remain essentially unchanging during the time of the calculation, making it reasonable to impose constant state boundary conditions there. (For safety, we put the outer boundary at $\sim 10^6 r_G$, where r_G is the Schwarzschild radius $r_G = 2GM/c^2$.)

The initial model, constructed by solving the stationary version of equations (1) – (5) for an optically thick medium, is thermally unstable according to the local stability criterion with the region of instability extending from $4.5 r_G$ to $17.5 r_G$. (This is slightly different from the HMK model which was locally unstable between $5.2 r_G$ and $13.1 r_G$.) Data from the stationary calculation was then transferred onto the finite difference grid used for the time-dependent calculation (as described in Paper I). Numerical noise resulting from this and from the nature of the finite-difference treatment was then sufficient to trigger growth of the instability.

After less than one second of the evolution, two density waves are sent out from around $6 r_G$ (within the locally-unstable region), one moving inwards and the other outwards. This can be seen in Figure 1, where the surface density Σ is plotted against r/r_G at a succession of times (marked in sequence from 1 to 11 with the dotted curve corresponding to the beginning of the cycle). The ingoing wave (see the curve labelled 1) propagates quickly, passes through the sound horizon (where the inward velocity is equal to the sound speed) and disappears

into the black hole, taking with it a significant amount of matter. This is shown in more detail in Figure 2. The outgoing wave is launched on its progress out through the disc only when the ingoing wave has fully passed in through the sound horizon.

At the onset of the instability, the temperature rises significantly in the unstable region (see the upper panel of Figure 3), increasing the contribution of the radiation pressure by nearly an order of magnitude. The first effect of this is to push the ingoing density wave into the black hole leaving behind an underdensity while causing just a small increase of density at the place from which the outgoing wave will be launched. As the outgoing wave progresses outwards (with the Mach number of the outflow v_r/c_s reaching values as high as 0.2 – see Figure 4) the temperature peak is reduced but remains at a level still well above that of the initial model. The outgoing wave heats the material through which it passes, causing the part of the disc internal to it to swell up as shown in Figure 5. Advective cooling is dominant in the region just behind the peak of the wave. (Note that the sound speed c_s used in Figure 4 and elsewhere is the local *isothermal* sound speed $(p/\rho)^{1/2}$ which is not exactly the quantity which is relevant for considerations of causal connection. The effective “sonic point” for these purposes comes *near* to the place where $v_r/c_s = -1$ but does not precisely coincide with it.)

In order for the outgoing wave to continue its propagation, it is necessary that the material behind it should remain in a hot state. Once the wavefront has moved beyond the linearly-unstable region, it becomes progressively harder for the temperature to be maintained in the high state and eventually the front starts to weaken and the temperature falls dramatically down to a low state well below that of the initial model (see curve 8). The front dies after about 20 seconds when it has reached about $100 r_G$ and a slow filling up of the under-dense region then begins, proceeding on the viscous timescale, with an associated progressive rise in temperature. Eventually, when the configuration has returned near to its initial state, a second cycle begins which is very similar to the first one. (There is a slight difference because the configuration does not pass exactly through the stationary state at the end of the cycle.)

These results were obtained with formulae treating the medium as always remaining optically thick. However, subsequent checking of the values of the effective optical depth ($\tau_{eff} = (\tau_R \tau_P)^{1/2}$) revealed that this does not always remain much greater than unity when the temperature is in the high state so that values for F^- obtained using expression (12) deviate significantly from those obtained with equation (9) which is appropriate for the

optically-thick limit. To check on the error introduced by this, we implemented the general treatment described in Section 2 and repeated the calculation. The overall behaviour was extremely similar and the only significant differences were related to small changes in the temperature profiles in the inner parts of the disc (see the lower panel of Figure 3). At the beginning of the second and subsequent cycles, the ingoing wave developed a shock as it propagated into the black hole (see Figure 6) whereas it remained regular when the medium was treated as optically thick. Note that the shock is in the supersonic part of the flow, inside the sound horizon.

As in Paper I, it is valuable here also to consider a local view of the results, taking cuts at particular values of r and seeing how the values of parameters there vary as the evolution proceeds. In particular, we concentrate on evolution in the phase plane obtained by plotting $\log T$ against $\log \Sigma$. If one plots points corresponding to parameter values at a specified value of r for a sequence of stationary models having the same α but progressively increasing values of the accretion rate \dot{M} , then characteristic S-shaped curves are obtained. In non-linear dynamics, existence of such S-shaped phase portraits of a system is an indication of possible limit cycle behaviour.

Figures 7, 8 and 9 show the phase portraits (upper panels) and temperature time series at $5 r_G$, $10 r_G$ and $50 r_G$ respectively. (There are only very small differences for these figures between the optically thick calculation and the one with the general treatment – the results presented here are from the optically thick calculation.) The location $5 r_G$ (Figure 7) lies just within the locally unstable region for the initial model (in which parameter values lie on the middle branch of the corresponding S-curves for stationary models) and the initial state is represented by point 0. The S-curve for this value of r is shown by the dotted line in Figure 7 (with the lower branch being covered by computed points which we will now discuss). After the onset of the instability, the subsequent behaviour follows a closed path in the phase plane, passing successively through the points labelled 1, 2, 3, etc., which correspond to the times for which the equivalently labelled curves were drawn in the earlier figures. Each cycle lasts for approximately 780 seconds and, as far as quantities at this location are concerned, can be divided into two main sections. The first is the outburst (for which a more detailed view of the temperature time series is shown in Figure 10). This commences with the temperature rising rapidly (points 1 and 2) and then falling again (point 3) while the surface density decreases by more than an order of magnitude. This initial part lasts for approximately one second. Following this, there is around 20 seconds of almost constant

temperature during which Σ first remains essentially constant and then starts to gradually increase again with the trajectory running parallel to the middle branch of the S-curve but not quite lying on top of it. This gradual change is terminated by a dramatic drop in temperature by a factor of three (point 8) down to the low-temperature state. This marks the end of the first (outburst) stage and the second (quiescent) stage then begins during which the evacuated inner part of the disc is slowly refilled (on the viscous timescale). This starts with a continuing slow decrease in temperature, lasting for around 50 seconds, with the trajectory following the lower branch of the S-curve. Σ is *decreasing* during this time but the decrease is then reversed and the trajectory begins to move steadily up the lower branch (with rising T and Σ) for around 700 seconds until the turning point is reached and another outburst begins. The calculation was continued up to the beginning of the fourth cycle. The first cycle is indicated with the solid line, the second with squares (marking the data points plotted), the third with crosses and the fourth with triangles. The later cycles are essentially identical to each other after a small change from the first one. Figures 8 and 9 show the equivalent phase portraits and temperature time series for $10 r_G$ (within the locally-unstable region at the initial time) and $50 r_G$ (which is outside it).

4 DISCUSSION

To make it easier to compare our results with those of HMK, the curves shown in Figure 1 correspond to times chosen so as to have the front at similar locations to those shown in Figure 5 of their paper. Our curves labeled 1, 2, 3, 4, 5, 6 and 7 have the front at almost exactly the same positions as for their curves with the same numbers but the front propagates further out in our calculation and when it starts to break down (curve 8), it has reached around $100 r_G$ rather than $70 - 80 r_G$ as in their calculations. Our curves 9 and 10 are at roughly the same stages of the evolution as theirs.

Our results are strikingly similar to those of HMK and, since the numerical methods used in the two calculations were quite different, this provides a convincing confirmation of the results obtained by HMK and of the reality of the limit cycle behaviour. The main differences between our results and theirs are in the distance to which the front propagates (as mentioned above) and the amplitude of the density wave which is considerably greater in our calculation. These differences are, at least in part, due to the different mathematical formulation used (see Paper I and our comment earlier in this paper about the size of

the locally unstable region) but they can also be related to differences in the treatment of opacities and the diffusiveness of the numerical scheme (ours has extremely low intrinsic numerical diffusion). Another difference is that they find that the disc remains effectively optically thick throughout whereas we do not, although the difference produced by this is small. Also, we have explicitly shown that the behaviour repeats for a number of cycles with those after the first one being essentially identical.

In Paper I, where we studied in detail a low- α model ($\alpha = 0.001$) having a locally unstable region of roughly the same extent as that for the model treated in the present paper, we did not observe limit cycle behaviour and the run ended with formation of a velocity spike adjacent to the sonic point which appeared to be catastrophic. Now, using similar numerical techniques and mathematical formulation, we have found a completely different result for the high- α case and we need to ask why this happens. A key difference is that for high α , the sonic point in the stationary models is outside the location of the marginally stable orbit (at $3r_G$) whereas for low α , it is inside it. Figure 11 shows the behaviour of v_r/c_s plotted as a function of r/r_G for the two cases at successive times during the inward propagation of the disturbance produced when the thermal instability is initiated. The top panel shows the high- α case and the bottom panel is for low α . Consider first the high- α case. The initial profile of v_r/c_s , shown by the upper dashed curve, is distorted by the passage of the ingoing wave and progressively changes into the qualitatively different profile shown by the lower dashed curve which is then characteristic of the type of profile seen in the inner parts of the disc during the outward propagation of the outgoing wave. Note that the sonic point does not move inwards, remaining just external to $3r_G$, and that there is a striking pivot-like behaviour. (We recall here our earlier comment that the effective sonic point for considerations of causality does not precisely coincide with the point where $v_r/c_s = -1$ in these figures.) For low α , the first of the curves is the one shown with the dotted line and after a small initial excursion in the outward direction, the sonic point is then pushed substantially inwards with the profile steepening and then producing a peak with positive (outward) velocities, leading to the formation of the velocity spike shown in Figure 5 of Paper I which caused termination of the run. For high α , the ingoing wave proceeds unimpeded into the black hole and when this has happened, the outgoing wave is launched on its progress out through the disc as described earlier. For low α , however, the ingoing wave was stopped in its inward progress by the formation of the velocity spike and, while the beginnings of the

outgoing wave could be seen, the stage at which it could have been launched in its outward progress through the disc was never reached.

We have now made further refinements to the code which allow us to continue the low- α calculation beyond the previous termination point and it turns out that the growth of the velocity spike is not catastrophic after all but rather that the amplitude subsides again after reaching a maximum and the spike then keeps appearing and disappearing during the subsequent evolution. Since the precise nature of this further evolution seems to depend very much on how dissipative processes are treated, we will delay detailed discussion of it until our next paper in which we will study the effects of adopting a more physical viscosity prescription than the simple α law used here. However, we should report at this stage that by adding a large enough amount of artificial diffusion of a particular type, we have found it possible to suppress the effects of the velocity spike sufficiently so that an outward-going wave *is* successfully launched out through the disc, giving a limit-cycle behaviour very similar to that for the high- α case. We stress that this is an artificially-produced result obtained by adding a dissipative term in a way which we do not regard as being legitimate unless directly motivated by a physical argument. We regard the account given in Paper I as our definitive description of the low- α case within our present physical assumptions and mathematical formulation and stress that the appearance of the sonic-point velocity spike is part of a consistent picture based on a fundamental underlying difference between the low- α and high- α cases as discussed above. The calculation leading to it has been extensively tested, as described in Paper I. The interest of our new experiment with the added artificial diffusion lies in indicating that *if* real physical processes or improved mathematical description were to produce a similar effect to that of the artificial term which we introduced, then limit-cycle behaviour could still occur also for the low- α case. We will return to this discussion in the Conclusion.

Similar problems in understanding the physical nature of limit-cycle behaviour have already been encountered in the context of Keplerian discs. Taam & Lin (1984) found a limit cycle connected with radiation pressure driven thermal instability operating in Keplerian accretion discs around black holes and neutron stars. Later, it was recognized by Lasota & Pelat (1991) that this was an artificially-produced result obtained because of a particular treatment of the radiative cooling. They also pointed out that the real nature of the limit cycle ought to be investigated outside the thin disc approximation, as we are doing here,

taking into account departures from Keplerian motion and the transonic character of the flow.

5 CONCLUSION

In this paper, we have investigated the time evolution of a thermally unstable transonic accretion disc with a high value for the viscosity parameter $\alpha = 0.1$. We confirm the results obtained by Honma, Matsumoto & Kato (1991) who found evidence for limit-cycle behaviour for a similar model. We have continued our calculations for three complete cycles and have found a period of about 780 seconds.

The cycle can be divided into two distinct parts: an outburst phase and a quiescent one. During the outburst phase, the flow ceases to be optically thick in the inner part of the disc and we have implemented an appropriate treatment for this regime. The results were compared with those from a run in which the medium was treated as always being optically thick but only small differences were found, probably because τ_{eff} never becomes much smaller than unity.

The non-stationary behaviour found for the high- α model is significantly different from that for the low- α model presented in our earlier paper (Szuszkiewicz & Miller 1997), for which no limit-cycle behaviour was seen. The key difference concerns what happens when the ingoing wave reaches the sonic point. For high α , the location of the sonic point remains essentially fixed and the ingoing wave passes through it unimpeded and on into the black hole whereas for low α the sonic point was pushed inwards and a spike of positive velocity formed just outside it, stopping the inflow.

As outlined in Paper I, the strategy of the research programme, of which the present paper forms a part, was to study first the simple case of the original version of the slim-disc model, with all of its associated assumptions and approximations, and then to consider the results obtained for this as a standard reference against which to compare results from subsequent more elaborate calculations in which additional effects would be added one by one, thus giving a systematic way of understanding the contribution from each of them. The present paper goes beyond Paper I in considering a higher value of α but retains other simplifications such as the α viscosity prescription, neglect of other dissipative effects, assumption of hydrostatic equilibrium in the vertical direction, use of the pseudo-Newtonian potential. Our next step will include introducing a more physical viscosity prescription with

$\tau_{\varphi r} \propto \partial\Omega/\partial r$ which makes the crucial change of introducing a parabolic part into a system of equations which at present is purely hyperbolic. The effect of such dissipative terms can potentially be very important indeed.

Our basic numerical scheme is extremely non-diffusive. While it normally only requires the introduction of additional artificial viscosity in order to deal with shocks, there can also be other circumstances in which it is appropriate to introduce artificial diffusion, such as the one already described in Paper I. However, it has to be said that this is a delicate area forming part of the “black art” of numerical hydrodynamics which is not often discussed in the literature. When is the adding of artificial diffusion a benign thing, which allows one to smooth over shortcomings in the numerical or mathematical representation of the problem, and when does it become something drastic which changes the very nature of the problem? When we first tried to run the high- α case presented in this paper, we found that the outward-moving density wave was launched in exactly the way described here (a quite different behaviour from the low- α case) but that numerical stability broke down as the wave died at the far extent of its outward travel. We eventually cured this by introducing a particular form of artificial diffusion based on a prescription kindly supplied by F. Honma (private communication). Using an artificial term to help an already-dying feature to go quietly seems quite legitimate in view of the fact that it covers for the omission of real physical diffusive effects which would be included in a full treatment. On the other hand, using heavy artificial diffusion to neutralise the effect of the sonic-point velocity spike for low α , does *not* seem legitimate unless directly motivated by a physical argument. Maybe there *is* such a motivation and maybe there *is* genuine limit-cycle behaviour also for low α despite the fundamentally different behaviour at the sonic point. However, this remains to be seen when further relevant effects are included consistently in the calculations and the next stage of our work will be pointed in that direction.

ACKNOWLEDGMENTS

We gratefully acknowledge helpful discussions with Marek Abramowicz, Bożena Czerny, Gabriele Ghisellini, Fumio Honma, Andrew King, Jean-Pierre Lasota, Zbigniew Loska, Laura Maraschi, Derek Raine, Michał Różyczka, Marek Sikora, Roland Svensson and Andrzej Zdziarski. This work has been supported financially by the U.K. Particle Physics and Astron-

omy Research Council and the Italian Ministero dell'Università e della Ricerca Scientifica e Tecnologica.

REFERENCES

- Abramowicz M.A., Czerny B., Lasota J.-P., Szuszkiewicz E., 1988, *ApJ*, 332, 646
Artemova I.V., Bisnovatyi-Kogan G.S., Björnsson G., Novikov I.D., 1995, *ApJ*, 465, 119
Belloni T., Mendez M., King A.R., Van der Klis M., Van Paradijs J., 1997, *ApJ*, 479, L145
Honma F., Matsumoto R., Kato S., 1991, *PASJ*, 43, 147
Hubeny I., 1990, *ApJ*, 351, 632
Huré J.M., Collin-Suffrin S., Le Bourlot J., Pineau des Forets G., 1994, *A&A*, 290, 19
Lasota J.-P., Pelat D., 1991, *A&A*, 249, 574
Narayan R., Yi I., 1994, *ApJ*, 452, 710
Pringle J.E., Rees M.J., Pacholczyk A.G., 1973, *A&A*, 29, 179
Szuszkiewicz E., Miller J.C., 1997, *MNRAS*, 287, 165
Taam R.E., Lin D.N.C., 1984, *ApJ*, 287, 761

FIGURE CAPTIONS

Figure 1: Changes in the radial distribution of the surface density Σ (measured in units of g cm^{-2}) during the second evolutionary cycle. The curves marked 1 to 11 show the situation after 876.41, 876.45, 876.79, 877.20, 878.36, 880.12, 883.42, 893.0, 925.0, 985.1 and 1209.0 seconds respectively. The dotted line corresponds to the beginning of the cycle, at around 876 seconds, and the unmarked solid line in the lower panel (which is essentially coincident with the dotted one) is for the end of the cycle at 1657 seconds.

Figure 2: A more detailed view of the onset of the instability, showing the ingoing wave moving into the black hole and the subsequent launching of the outgoing wave. The surface density is plotted at a succession of times, with the dashed curves showing the profiles at the first and last of these times (the first one being the upper curve at small r .) The time elapsed between the first of the solid curves (when the perturbation is first apparent) and the last of the solid curves (when the outgoing wave is fully launched) is 0.14 seconds.

Figure 3: Evolution of the temperature profile in the calculation where the medium is treated as always being optically thick (upper panel) and in the calculation where regions which are not optically thick are treated in the different way described in the text (lower panel). The temperature T is measured in degrees Kelvin and the labels correspond to the same times as in Figure 1.

Figure 4: The profile of the Mach number plotted for the same times as in Figure 1. Note the marked change in the shape of these curves between the initial time (marked with the dotted curve), for which there is a sharp “elbow” in the curve near to the sonic point, and the later times when there is a gently changing slope behind the outgoing wave.

Figure 5: The half-thickness of the disc (in units of r_G) plotted as a function of r/r_G for some of the times shown in Figure 1.

Figure 6: Formation of a shock in the ingoing wave at the beginning of the second cycle in the calculation where the medium was not treated as if it were always optically thick. The Mach number is plotted against r/r_G at a succession of times with the dashed curve being the first. The time elapsed between the first and last curves is about 2 milliseconds. The grid spacing seen in this very expanded picture may appear to be rather coarse but we note that it was, in fact, quite adequate for following the shock propagation shown which, in any case, is entirely inside the sound horizon and hence does not affect the parts of the solution further out.

Figure 7: The phase portrait in the $\log T - \log \Sigma$ plane (upper panel) and the temperature time sequence (lower panel) for $5 r_G$. The time t is measured in seconds.

Figure 8: The phase portrait in the $\log T - \log \Sigma$ plane (upper panel) and the temperature time sequence (lower panel) for $10 r_G$.

Figure 9: The phase portrait in the $\log T - \log \Sigma$ plane (upper panel) and the temperature time sequence (lower panel) for $50 r_G$.

Figure 10: Expanded view of the temperature time sequence for $5 r_G$ during the initial outburst.

Figure 11: Comparison between the Mach number evolution for the high- α model (upper panel) and the low- α model (lower panel). The elapsed time is much greater for the low- α case than for the high- α one (~ 180 seconds as compared with ~ 1 second). This is related to the difference between the thermal timescales in the two cases.

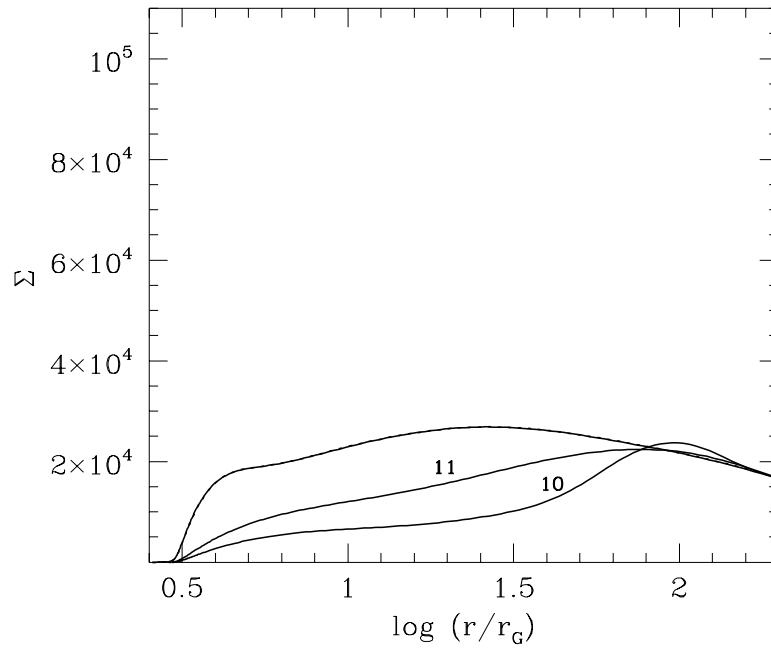
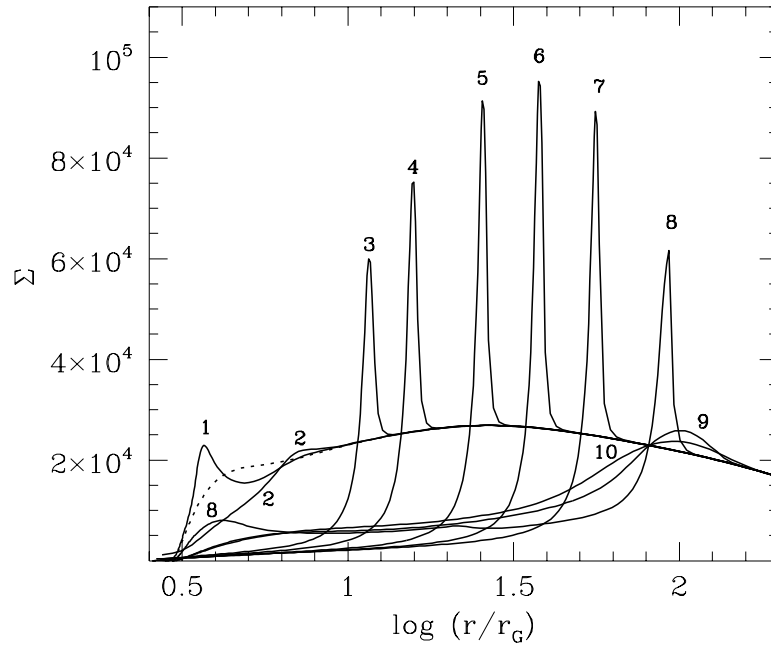


Figure 1

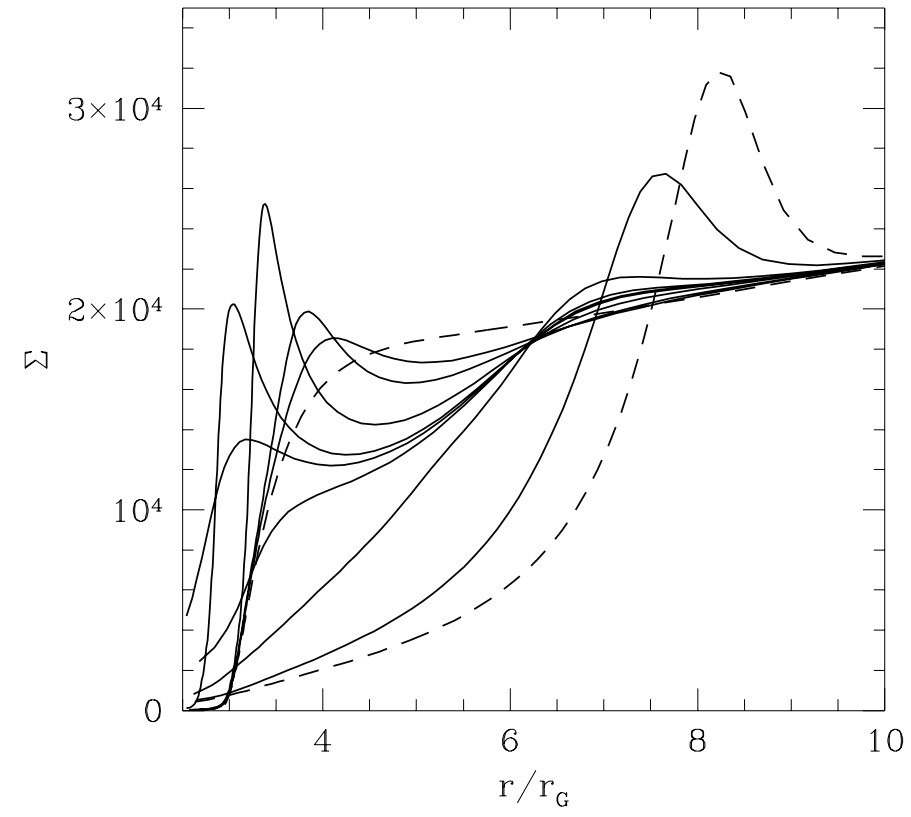


Figure 2

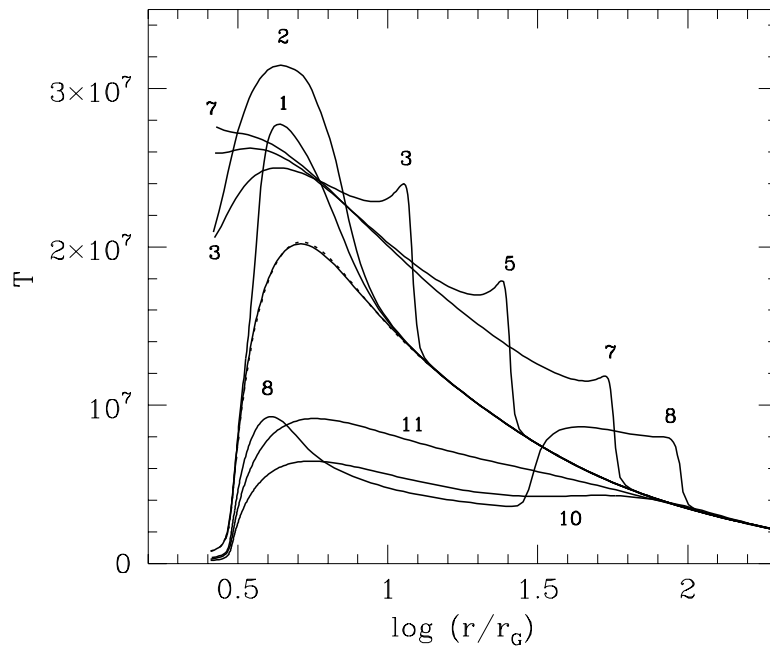
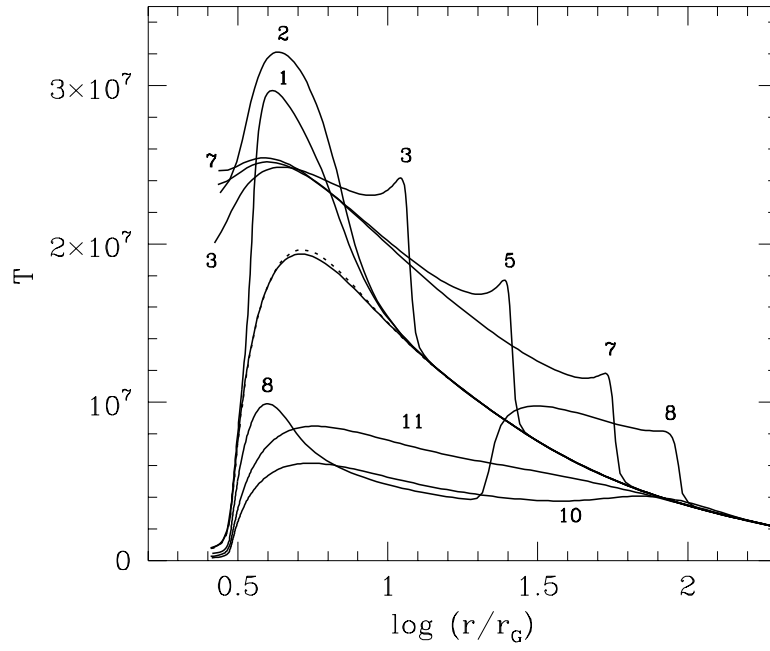


Figure 3

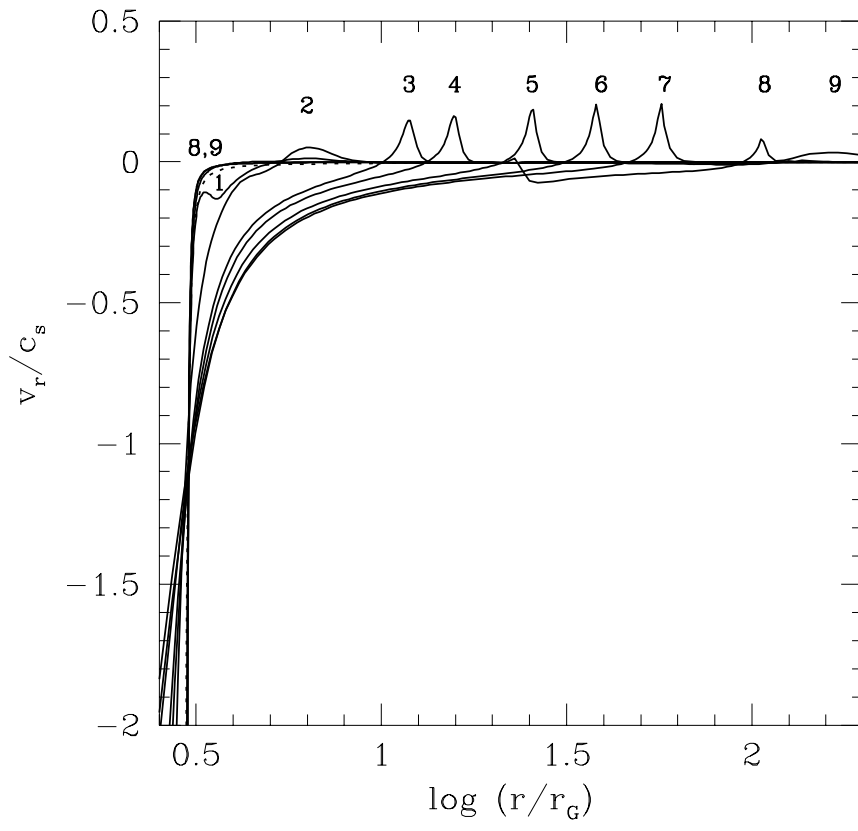


Figure 4

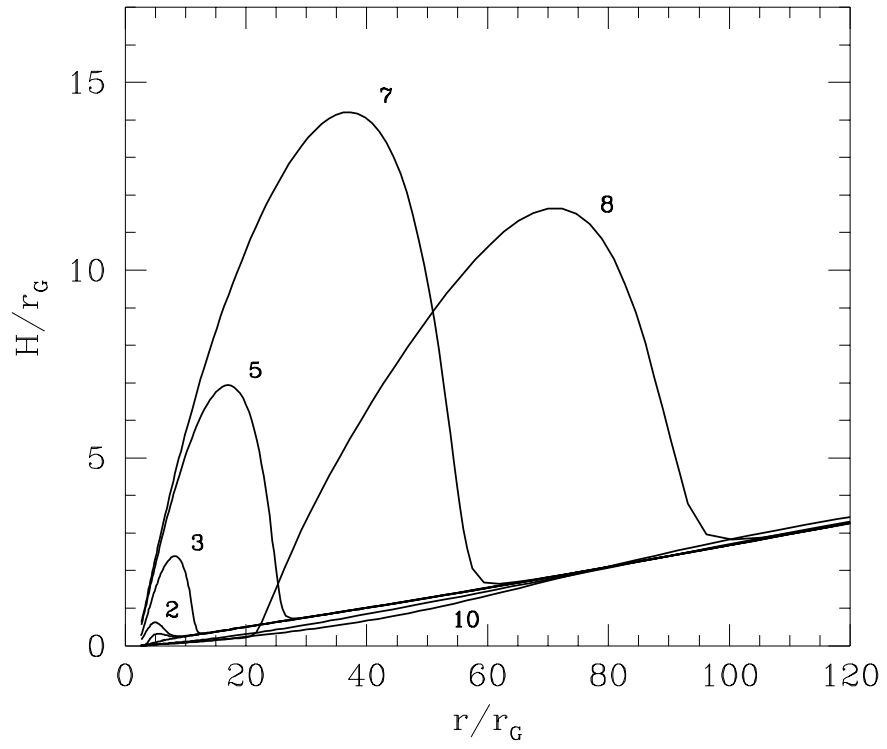


Figure 5

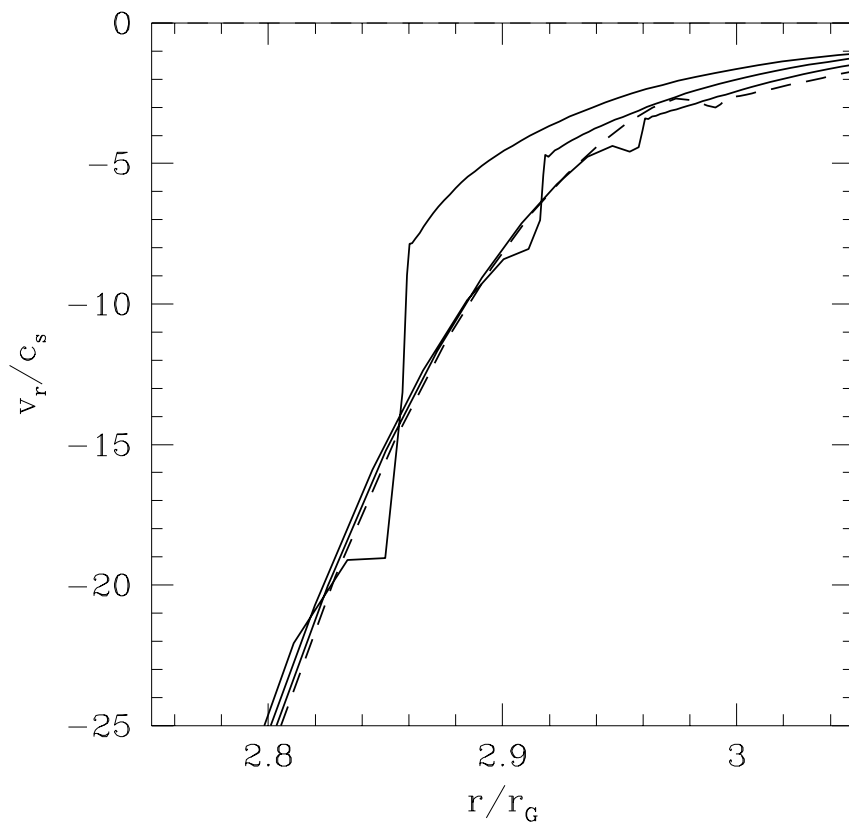


Figure 6

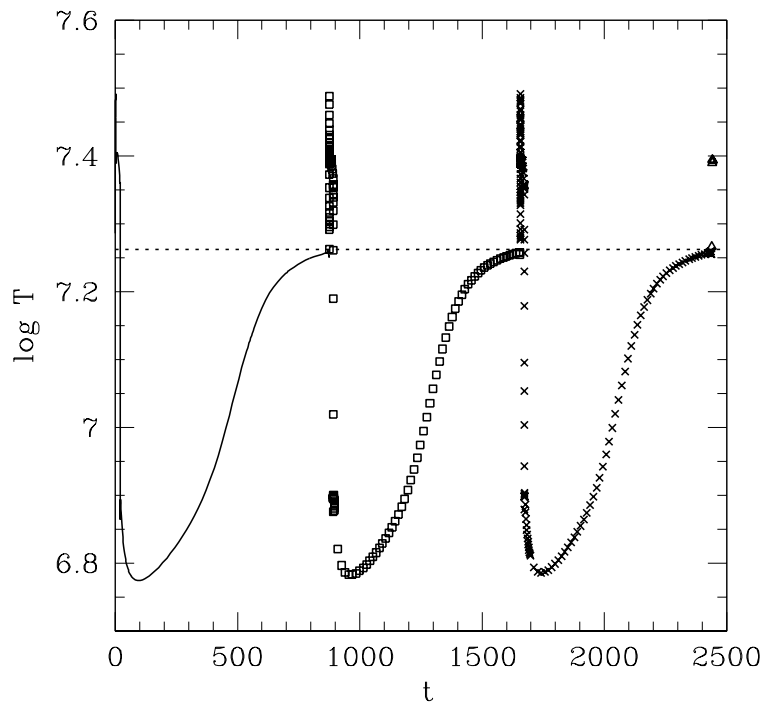
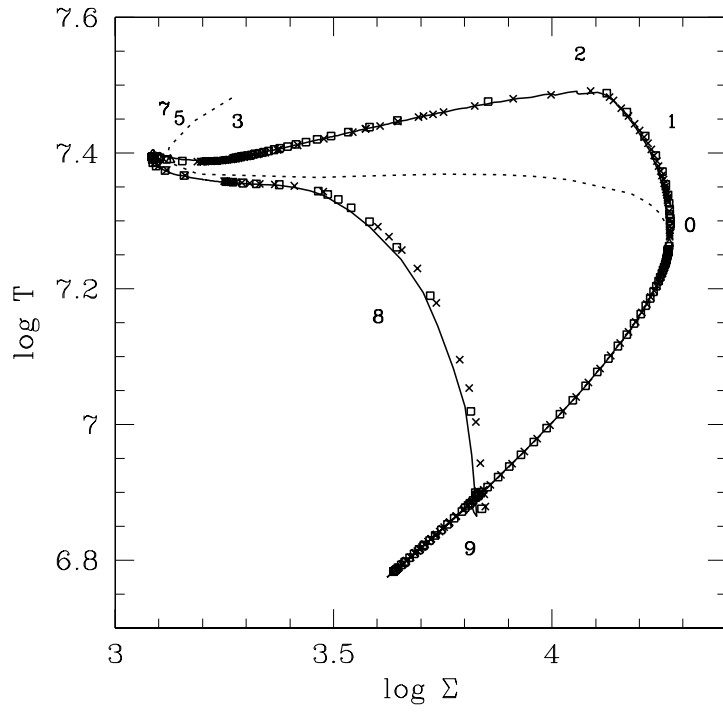


Figure 7

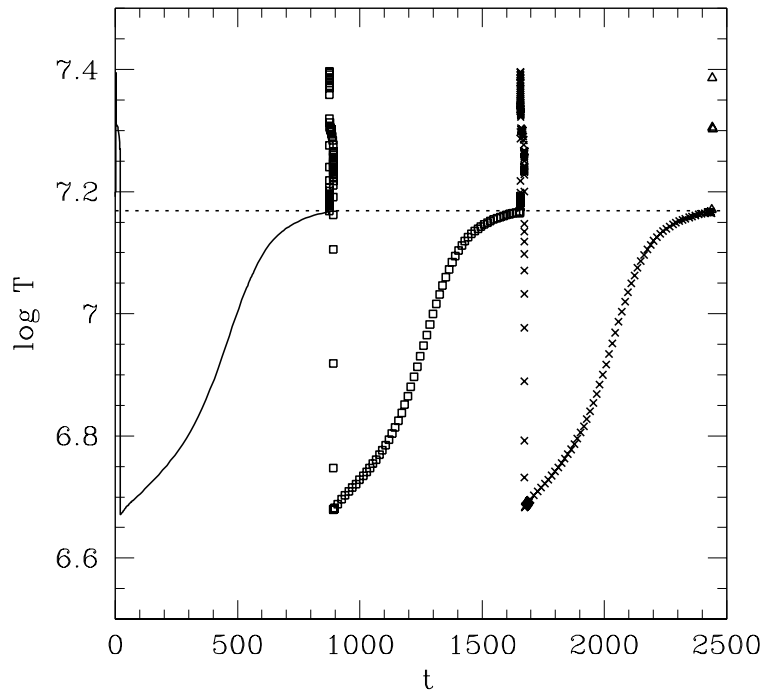
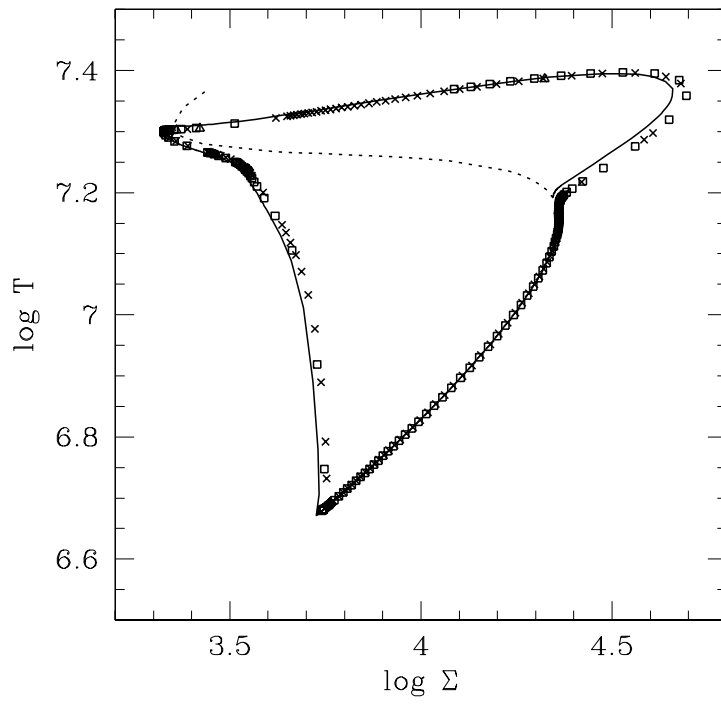


Figure 8

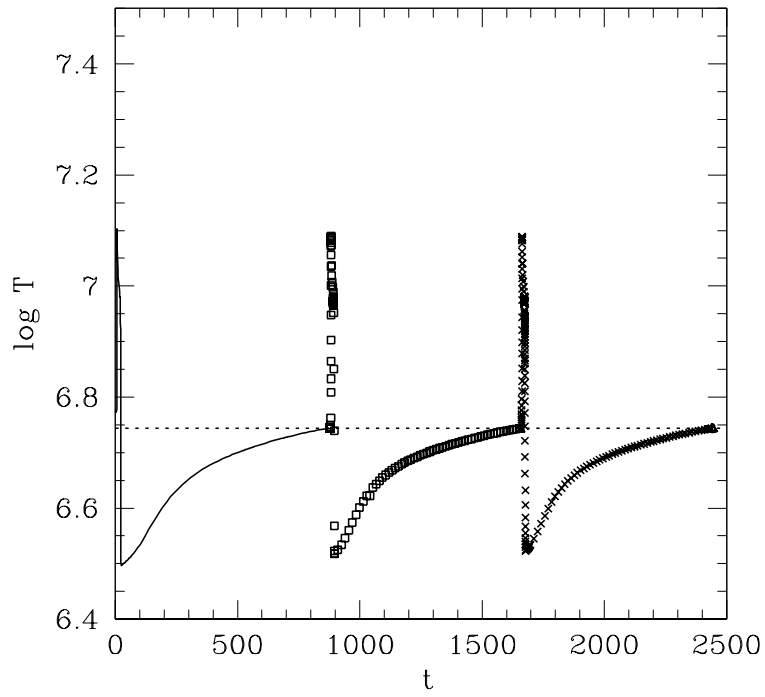
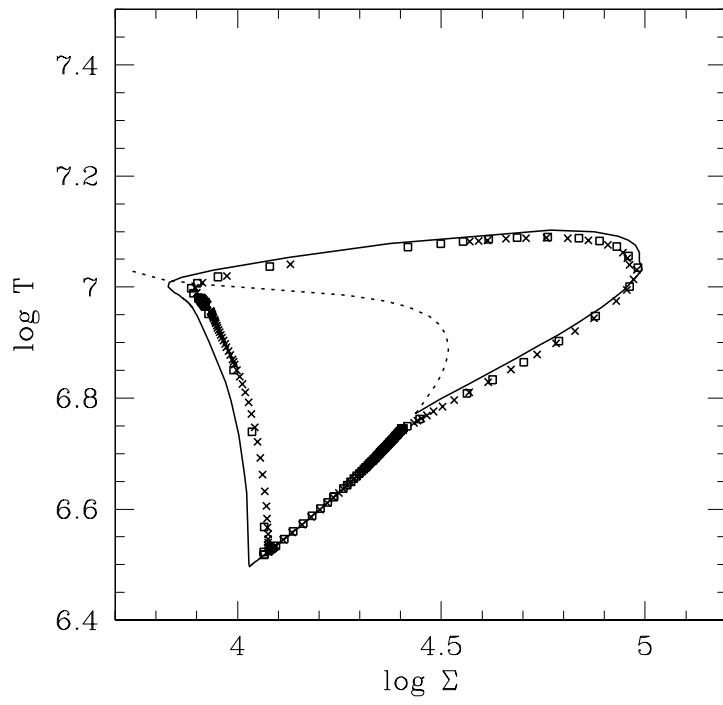


Figure 9

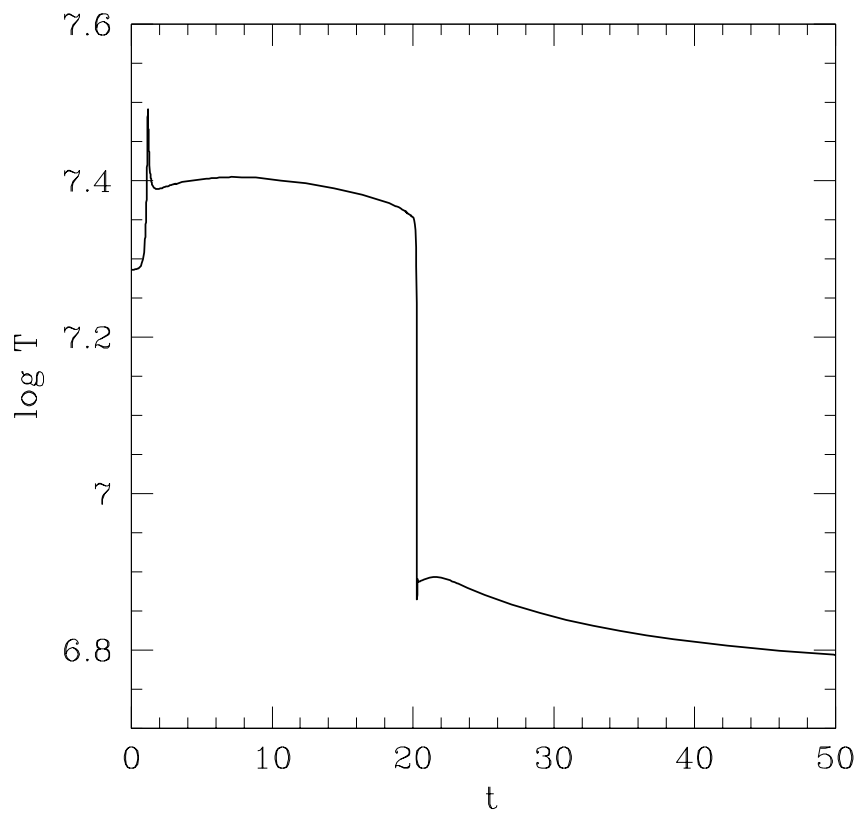


Figure 10

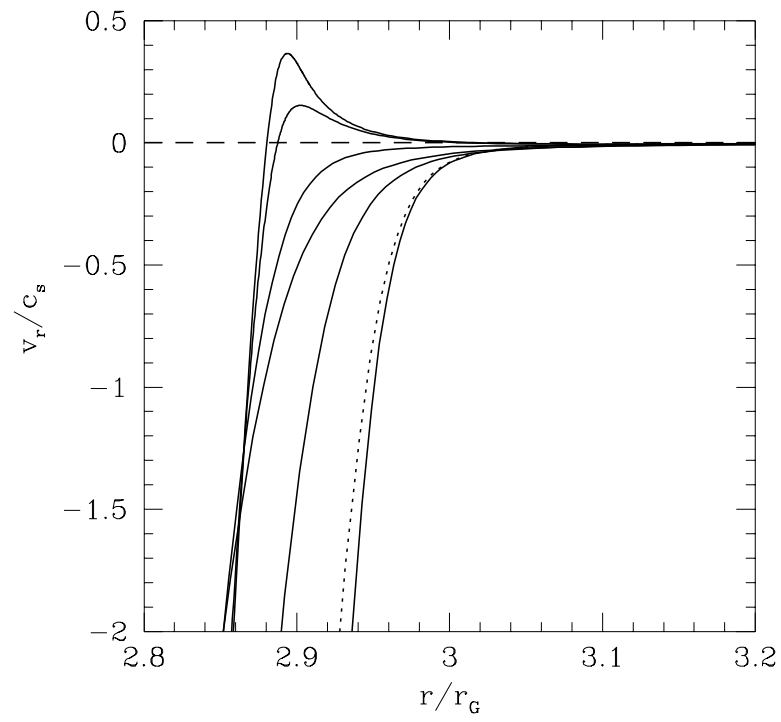
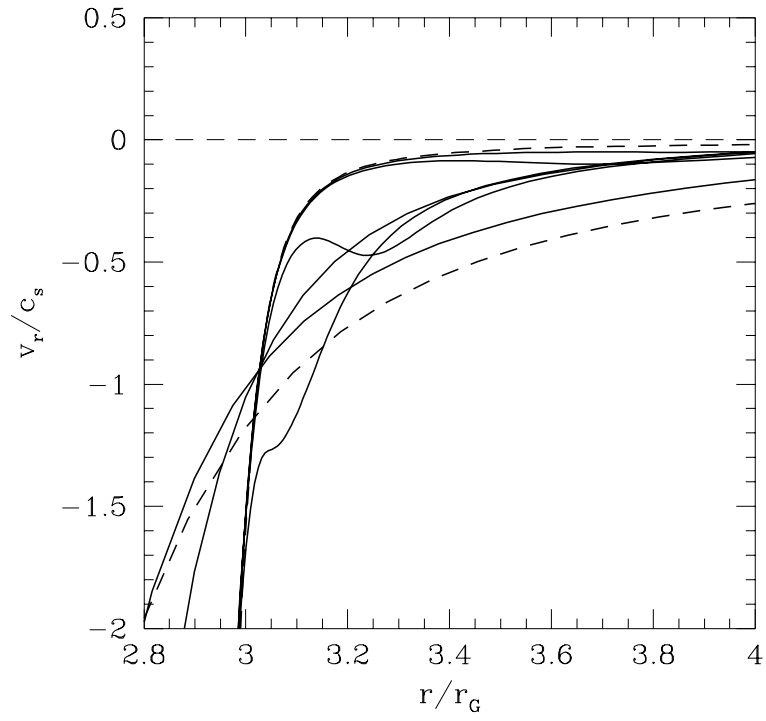


Figure 11